CADRILLE: MULTIMODAL CAD RECONSTRUCTION WITH REINFORCEMENT LEARNING

Anonymous authors

Paper under double-blind review

ABSTRACT

Computer-Aided Design (CAD) plays a central role in engineering and manufacturing, making it possible to create precise and editable 3D models. Using a variety of sensor or user-provided data as inputs for CAD reconstruction can democratize access to design applications. However, most existing methods focus on a single input modality: point clouds, images, or texts, which limits their generalizability and robustness, while few multimodal approaches struggle to deliver competitive quality. Leveraging advances in vision-language models (VLM), we propose cadrille, a multimodal CAD reconstruction model that takes inputs of three modalities and outputs executable Python code for CAD reconstruction. Inspired by large language model (LLM) training paradigm, we adopt a two-stage pipeline: supervised fine-tuning (SFT) on large-scale procedurally generated data, followed by reinforcement learning (RL) fine-tuning using online feedback, obtained programatically. In the DeepCAD benchmark, our SFT model outperforms existing single-modal approaches in all three input modalities simultaneously. More importantly, after RL fine-tuning, cadrille sets new state-of-the-art in as many as 10 benchmarks across three modalities and four datasets, including a real-world one.

1 Introduction

Computer-Aided Design (CAD) is the core of modern engineering and manufacturing, providing the tools to create detailed and modifiable 3D models (Briere-Cote et al., 2012). Creating CAD models manually requires skills, time, and effort. To simplify this process, CAD reconstruction aims at generating CAD models directly from scanned objects, making the process faster, cheaper, and overall more accessible (Rukhovich et al., 2024).

Typically, CAD models are created with a sequence of 2D sketches and 3D operations (Willis et al., 2021; Wu et al., 2021). This representation allows CAD models to be easily edited, making it prevalent in popular CAD tools like SolidWorks and AutoCAD and in CAD generation research. Most existing CAD generation methods define CAD sequences using special command tokens (Khan et al., 2024a; Wu et al., 2021). However, state-of-the-art results are obtained via mapping CAD sequences to casual Python code (Rukhovich et al., 2024). Following the same paradigm, we generate CAD models as executable Python scripts.

The most well-studied input modality in CAD reconstruction is naturally a point cloud (Rukhovich et al., 2024). However, point clouds can only be obtained when a physical 3D object is available, while scanning usually requires special equipment, making the process complicated for non-experts. Images capture finer details and can be sourced using customer low-end devices (e.g., smartphone cameras), hence relaxing the hardware requirements (Chen et al., 2025; 2024). In the meantime, textual descriptions can enrich the object representation with semantic context (Khan et al., 2024b). Using various input modalities, such as multi-view images, or natural language descriptions, would make design assistance applications simple even for non-experienced users. Recent emergence of vision-language models provides a solid ground for multimodal CAD reconstruction. However, the first multimodal methods in that vein (Xu et al., 2024b; Wang et al., 2025b) are dramatically inferior to single-modal approaches, so the full potential of VLMs for CAD reconstruction is yet to be unleashed.

056

058

060

061 062

063

064

065

066

067 068 069

070

071

072

073

074

075

076

077

078

079

081

083

084

087

090

092

093

094

096 097

098

099

100

101

102

103

104

105

106

107

Figure 1: Compared to state-of-the-art CAD-Recode, the only existing method that converts point clouds into Python code, <code>cadrille</code> has two key novelties. First, it goes beyond the standard training scheme and adapts LLM RL fine-tuning for CAD reconstruction (left). Moreover, besides point clouds only accepted by single-modal CAD-Recode, <code>cadrille</code> extends to images and textual descriptions, making it the first multimodal approach delivering state-of-art results (right).

Existing CAD reconstruction methods face generalization issues due to how they are trained. Specifically, handcrafted CAD datasets are small and limited in diversity (Khan et al., 2024a), while models trained with procedurally generated data struggle to transfer to the real-world domain (Rukhovich et al., 2024). In the vein of the standard LLM training pipelines (Shao et al., 2024), Chen et al. (2025); Wang et al. (2025a); Guan et al. (2025) bring RL fine-tuning into the CAD reconstruction context. However, all of them perform both supervised and RL fine-tuning on the same dataset, which does not help bridging the gap between training and testing data. In contrast, we use voluminous procedurally generated data for supervised training, while valuable but scarcer handcrafted data is reserved for RL fine-tuning. This scheme eliminates the need for large-scale handcrafted data and allows the model to first generalize across the CAD domain and then specialize using preference-based objectives.

Our experiments show that cadrille outperforms existing modality-specific baselines in accuracy. Moreover, RL fine-tuning ensures validity of generated Python code, which posed a challenge for prior works. As a result, the proposed approach demonstrates impressive robustness and sets a new state-of-the-art on several CAD datasets, including a real-world CC3D (Mallis et al., 2023). Essentially, this opens up new possibilities for generalization in open-world scenarios.

In summary, our contributions are as follows:

- We present cadrille, an LLM-based model able to process point clouds, images, and textual inputs, and generate Python scripts for CAD reconstruction;
- We are the first to prove that RL fine-tuning improves multimodal CAD reconstruction;
- With a single model, we simultaneously achieve state-of-the-art results across three input
 modalities (point clouds, images, texts) and four datasets (DeepCAD, Fusion360, CC3D,
 Omni-CAD), a total of 10 benchmarks, making it the most comprehensive evaluation of
 CAD reconstruction methods up-to-date.

2 RELATED WORK

CAD Generation Existing CAD generation methods can be classified into three categories based on CAD model representations: constructive solid geometry (CSG) (Du et al., 2018; Sharma et al., 2018; Nandi et al., 2018; Ellis et al., 2019; Tian et al., 2019; Friedrich et al., 2019; Kania et al., 2020; Ren et al., 2021; Yu et al., 2022; 2023), boundary representation (B-rep) (Wang et al., 2020; Sharma et al., 2020; Lambourne et al., 2021; Wang et al., 2022; Guo et al., 2022; Jayaraman et al., 2023; Liu et al., 2024a;b; Xu et al., 2024c; Li et al., 2025b) and CAD sequence (Wu et al., 2021; Lambourne et al., 2022; Ren et al., 2022; Xu et al., 2022; 2023; Zhang et al., 2025b; Badagabettu et al., 2024; Chen et al., 2024; Khan et al., 2024a;b; Ma et al., 2024; Mallis et al., 2024; Li et al., 2025a; Doris et al., 2025; He et al., 2025; Yuan et al., 2025; Wang et al., 2025b). In the CSG (Foley, 1996) paradigm, CAD is represented as a CSG tree constructed using boolean operations (union, subtraction, difference) of geometric primitives (e.g., cubes, cylinders, or spheres). This approach fails to express intricate shapes and is generally not well-aligned with how engineers and designers actually

build CAD models. B-rep (Ansaldi et al., 1985) is a graph that describes connections between faces, edges, and vertices of a 3D model. Creating a B-Rep requires enforcing topological consistency on edges, which introduces additional complexity to the generation procedure and complicates editing of generated models.

CAD Sequence Reconstruction Unlike general CAD generation, which may prioritize plausibility, diversity, or creativity in design, CAD reconstruction aims at faithfulness to the given inputs, requiring the output model to match the original shape.

Point clouds are the most well-studied input modality in CAD reconstruction. The seminal work on point cloud-based CAD reconstruction by Wu et al. (2021) proposed encoding CAD sketch-and-extrude sequences as special tokens. Beyond that, DeepCAD, a large-scale dataset of 180k hand-crafted CAD models, was presented. Subsequent works (Dupont et al., 2024; Khan et al., 2024a; Xu et al., 2023) adopted the same CAD representation and trained on the same DeepCAD dataset. More recently, CAD-Recode (Rukhovich et al., 2024) introduced a paradigm shift by representing CAD models as Python code, providing greater expressiveness and flexibility, and released a new dataset of approx. 1 million procedurally generated CAD models.

Only few recent works (Chen et al., 2024; Khan et al., 2024b; Wang et al., 2025c; Chen et al., 2025) have explored CAD reconstruction from alternative input modalities, such as single- or multiview images and natural language descriptions. These approaches extend the DeepCAD dataset by rendering synthetic views or generating textual captions for existing CAD models. Among them, CADCrafter (Chen et al., 2025) stands out for its unified framework that handles both single- and multi-view inputs, whether rendered or real. The seminal Text2CAD (Khan et al., 2024b) uses a vision-language model (VLM) to generate detailed captions for DeepCAD shapes and then trains a model to predict CAD sequences from those textual descriptions. Its recent follow-ups (Xie & Ju, 2025; Govindarajan et al., 2025; Guan et al., 2025; Wang et al., 2025a) adapted large language models for text-based CAD reconstruction.

Generally, state-of-the-art CAD reconstruction approaches are tailored to process specific input modalities with distinct architectures, while multimodal CAD reconstruction remains relatively underexplored. Recent CAD-GPT (Wang et al., 2025b) predicts a CAD model given a single image and textual description, while CAD-MLLM (Xu et al., 2024b) pioneers three-modal CAD reconstruction, yet both these methods fall behind single-modal state-of-the-art results (Rukhovich et al., 2024; Khan et al., 2024b; Chen et al., 2025) by a large margin (up to two orders of magnitude!). This makes our cadrille the first multimodal CAD reconstruction approach handling point clouds, images, and texts within a unified framework, that outperforms single-modal top-performing methods.

RL for CAD Reconstruction Reinforcement learning is used for CAD reconstruction from images (Sharma et al., 2018; Chen et al., 2025; Zhang et al., 2025a), and from B-Rep (Yin et al., 2025). Recent LLM-based CADFusion (Wang et al., 2025a) and CAD-Coder (Guan et al., 2025) address CAD reconstruction from texts, both performing supervised and RL fine-tuning on the same Deep-CAD dataset. On the contrary, we investigate RL fine-tuning for multimodal CAD reconstruction and improve the reconstruction quality by using large-scale procedurally generated data for SFT.

3 CAD SEQUENCE RECONSTRUCTION

Problem Formulation The task of CAD reconstruction implies recovering a CAD model given a multimodal input q, which can be a 3D point cloud, a set of images, or a textual description. We represent CAD models as Python scripts (Rukhovich et al., 2024) that, when executed, generate a parametric Boundary Representation (B-Rep) of a 3D shape. Respectively, given an input q, we search for a trainable policy π_{θ} , s. t. $\pi_{\theta}(q)$ produces a token sequence τ , which is essentially a text of a Python program generating a CAD model.

Multimodal Data For training a model, we derive all input modalities from ground-truth CAD models (Fig. 2). Below, we describe how each modality is constructed according to the established data generation protocols (Chen et al., 2025; Khan et al., 2024b; Wu et al., 2021).

Given a CAD model as a parametric 3D shape (B-Rep), we sample points directly from the parametric surfaces of the model. Modern CAD engines provide built-in routines for surface sampling, making it simple and straightforward.

To generate images, the B-Rep is first tessellated, i.e., converted into a triangle mesh that approximates the surface geometry. Then, this mesh can be rendered from multiple viewpoints to produce multi-view image inputs.

Generating textual data is notably more challenging. Since our goal is accurate geometry reconstruction rather than generating a semantically relevant sample, inputs should provide detailed and comprehensive geometric information. Consequently, loose textual descriptions

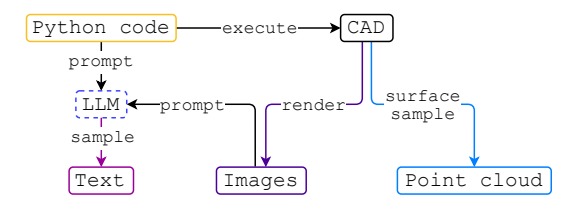


Figure 2: Overview of multimodal data generation pipeline producing textual descriptions, multiview images and point clouds.

are generally insufficient. The necessary level of granularity is investigated in Text2CAD (Khan et al., 2024b), where LLMs and VLMs are combined in a multi-stage sophisticated pipeline that generates textual descriptions from both the CAD sequence and rendered images.

4 Proposed Method

4.1 CADRILLE ARCHITECTURE

The cadrille architecture is depicted in Fig. 3. The model accepts inputs in the form of a point cloud, a set of images, or a text prompt, and outputs a Python code, that, when executed, produces a CAD model. cadrille is build on top of a VLM that natively supports text and image inputs and is already capable of generating Python code. Textual input is passed through the original embedding layer, and images are processed with an original visual encoder. The point cloud processing logic is the same as in CAD-Recode. Specifically, we use a single projection layer to embed 3D points, sample points from the surface via furthest point sampling, and do not use normals.

4.2 Supervised Fine-tuning

As shown on Fig. 1, cadrille benefits from three stages of training. First, we use VLM which is pre-trained on the internet-scale data in the unsupervised manner. After this stage, VLM is able to process textual and visual inputs and generate Python code, but lacks mechanisms to handle point clouds. In this work, we do not perform any unsupervised VLM training, but enjoy the capabilities of an already trained model.

The second stage is supervised fine-tuning for a specific task. During SFT, a model develops the ability to process point clouds and learns a policy π_{θ} to map multimodal inputs q to Python codes τ , making SFT an essential part of cadrille pipeline. We construct a training dataset \mathcal{D} of samples (q, τ) , where q is a multimodal input. The training procedure aims to minimize cross-entropy between ground truth and predicted Python code tokens:

$$\mathbb{E}_{(q,\tau)\sim\mathcal{D}}\left[\log \pi_{\theta}(\tau\mid q)\right]$$

4.3 LIMITATIONS OF SFT

Two-stage training has already been adopted in CAD-Recode, which employs supervised fine-tuning (SFT) to adapt a pretrained language model for point cloud-based CAD reconstruction. However, this strategy reveals its limitations in a cross-domain scenario: CC3D IoU is as low as 60% and the invalidity ratio (IR) is to 10%, which means that every tenth prediction fails to produce a valid output (Tab. 3, row 2). To mitigate this issue, CAD-Recode uses a test-time sampling technique. For each input query, 10 candidate Python programs are generated, and the candidate with the highest IoU is selected. After that, IoU increases to 74%, while IR drops below 0.5%. However, this improvement comes at the cost of a 10x increase in inference time. Can similar gains be achieved without sacrificing test-time efficiency?

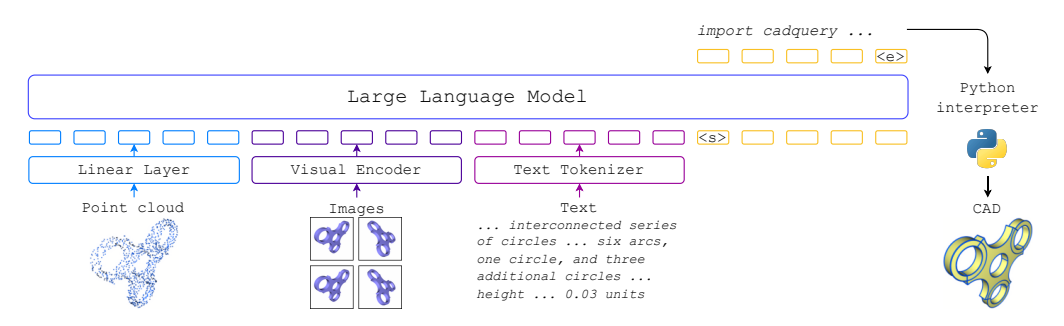


Figure 3: Overview of cadrille. It can handle three input modalities within a unified framework. Point clouds are processed with a trainable projection layer, while images and texts are passed to a VLM directly. The output of the model is an executable Python script for CAD generation.

To maintain fast and simple inference, we shift our focus to improving the training process. Training solely on procedurally generated CAD data might limit performance in real-world applications. Nevertheless, training on handcrafted models also presents challenges, e.g., Rukhovich et al. (2024) shows that SFT directly on the DeepCAD dataset harms performance, leading to a 10% drop in IoU.

Our experiments confirm that simply mixing procedurally generated and handcrafted data for training fails to improve results and can even degrade performance (Tab. 3, row 4). We attribute this to inconsistency in CAD sequences across datasets: for instance, DeepCAD models are constructed using commands like extruded cuts and symmetric extrusions, which are not present in the generation procedure of the CAD-Recode dataset.

To address this limitation, we introduce a novel third stage in the training pipeline, namely, reinforcement learning fine-tuning on handcrafted data not annotated with CAD sequences. This approach resolves inconsistency issues while still allowing the model to adapt to real-world domain.

4.4 RL FINE-TUNING

We formulate RL fine-tuning as follows. Given a dataset of inputs (either images or point clouds) $\mathcal{D} = \{q_i\}_{i=1}^N$, and reward function $R(\tau)$, we learn LLM policy $\pi_{\theta}(\tau \mid q)$ that generates a Python code τ for an input q, s.t. it maximizes the expected reward $\mathbb{E}_{q_i \sim D, \tau_i \sim \pi_{\theta}(\cdot \mid q_i)}[R(\tau_i)]$.

Note that at this stage annotated pairs of (q,τ) are not needed for supervision, since Python codes τ are being sampled from the trained SFT model. In fact, **CAD sequences are not needed for RL fine-tuning**, and the data requirements can be relaxed to 3D meshes instead. This is especially beneficial from the practical perspective, as RL fine-tuning can be performed using generally more accessible mesh datasets, which opens new possibilities for training models accommodated to artifacts present in real-world data.

The reward function $R(\tau)$ is a combination of terms that address precision and robustness:

$$R(\tau) = r_{\text{IoU}}(\tau) + r_{\text{invalid}}(\tau),$$

where $r_{\rm IoU}$ is an IoU between the CAD model produced by τ and ground truth 3D mesh, additionally multiplied by a factor of 10 to enforce precise reconstruction. $r_{\rm invalid}$ penalizes invalid predictions: it is set to -10 for invalid τ and 0 otherwise.

Empirically, we found that hard example mining leads to a faster convergence of RL fine-tuning. Consequently, we only use examples q where the reward $R(\tau)$ averaged over three samples produced by the SFT model is less than $R_{\rm th}$, where $R_{\rm th}=7.5$.

DPO Direct Preference Optimization (DPO) Rafailov et al. (2023) learns from pairwise preference data, approximating an implicit reward via a reparameterized Bradley-Terry model.

We construct the training dataset by sampling K = 5 Python codes τ for each input q from the SFT model π_{θ_n} . At each training step for the given sample, we randomly select two outputs. The output

with a larger reward $R(\tau)$ is considered to be a preferred prediction τ_w , and another is non-preferred τ_l . The optimization objective is formulated as:

$$\mathbb{E}_{(q,\tau_{w},\tau_{l}) \sim \mathcal{D}} \left[\log \sigma \left(\beta \log \frac{\pi_{\theta_{t}}(\tau_{w} \mid q)}{\pi_{\theta_{r}}(\tau_{w} \mid q)} - \beta \log \frac{\pi_{\theta_{t}}(\tau_{l} \mid q)}{\pi_{\theta_{r}}(\tau_{l} \mid q)} \right) \right]$$

DPO training starts with π_{θ_r} and proceeds for 10 epochs. After that, the SFT model is replaced with the latest π_{θ_t} , and trained for another 10 epochs. In this way, the model gradually diverges from the original SFT model. In our experiments, we found it to be beneficial for performance.

However, DPO performance is upper-bounded by the quality of the best generated sample for a given example. This limitation cannot be overcome without generating additional samples, so we adapt an online RL approach that can benefit from newly generated samples.

Dr. CPPO We combine two recent modifications of the GRPO: Dr. GRPO Liu et al. (2025b) which eliminates the need for a reference model and modifies the objective, and CPPO Lin et al. (2025) which uses samples with the strongest signal. The hybrid approach ensures both computational efficiency and accuracy; hereinafter, it is referred to as Dr. CPPO.

G sequences $\{\tau_g\}_{g=1}^G$ are sampled from the current policy $\pi_{\theta_{\text{old}}}(\tau \mid q)$ for a given input q with temperature T=1.0. For each output g, the advantage A_g is estimated as $A_g=r_g-\text{mean}(\{r_i\}_{i=1}^G)$. N samples with the highest $|A_g|$ are used to form a batch $\mathcal B$ and perform policy update by maximizing PPO Schulman et al. (2017) objective:

$$\mathbb{E}_{\left\{\tau_g\right\}\sim\mathcal{B}}\left[\min\left(\frac{\pi_{\theta_t}(\tau_g\mid q)}{\pi_{\theta_{\text{old}}}(\tau_g\mid q)}A_g, \; \operatorname{clip}\left(\frac{\pi_{\theta_t}(\tau_g\mid q)}{\pi_{\theta_{\text{old}}}(\tau_g\mid q)}, \; 1-\epsilon, \; 1+\epsilon\right)A_g\right)\right]$$

5 EXPERIMENTS

Datasets DeepCAD (Wu et al., 2021) (denoted as D in Tables) serves as our primary benchmark for supervised training. We adopt the Text2CAD version of DeepCAD, which enriches it with textual descriptions. The train set comprises approximately 160k samples, while 8046 are left for testing.

For SFT, we also use the procedurally generated CAD-Recode (Rukhovich et al., 2024) dataset (denoted as R in the tables). It is an order of magnitude larger than DeepCAD, consisting of approximately 1 million CAD programs written in CadQuery (Authors, 2024), a parametric Python-based CAD language.

Fusion360 (Willis et al., 2021) (denoted as F) is a small CAD reconstruction benchmark with complex and realistic CAD models. In the standard evaluation protocol, only the test split (1725 samples) is used, as absence of Python CAD sequences makes it unsuitable for conventional supervised training. Still, we can use its train set (6900 samples) for our annotation-free RL fine-tuning.

To show the versatility and applicability of our approach, in addition to handcrafted and procedurally generated meshes, we report metrics on the real-world CC3D dataset (Mallis et al., 2023) (denoted as C). It contains 2973 point clouds sampled from scans of CAD models with noisy values, missing parts, and smoothed edges.

Omni-CAD (denoted as O) presented in the CAD-MLLM paper (Xu et al., 2024b) is a large-scale dataset of handcrafted CAD models, sourced from the web. We evaluate on its test split composed of over 27K samples, and report results in Appendix B.

Metrics Following CAD-Recode, we evaluate the quality of the predicted CAD models using three metrics: Chamfer Distance (CD), Intersection over Union (IoU), and Invalidity Ratio (IR). Since invalid CAD models introduce a notable bias into mean estimates, we report both mean and a more robust median CD, both computed using 8192 points. CD values are multiplied by 10³. The divergence between ground truth and reconstructed meshes is measured using IoU (in %). The IR indicates the percentage of generated sequences that do not produce a valid CAD model.

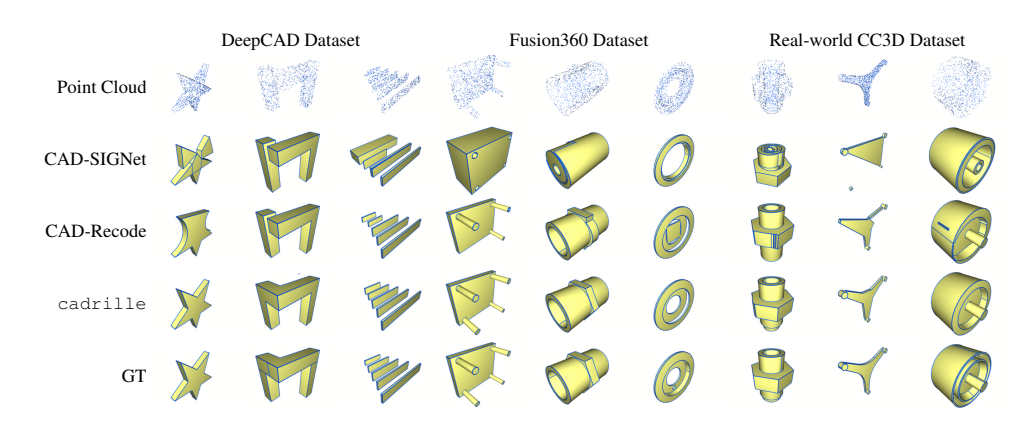


Figure 4: CAD models reconstructed from point clouds from the DeepCAD, Fusion360, and CC3D datasets.

5.1 Supervised Fine-Tuning

Results on DeepCAD In Tab. 1, we compare cadrille with single-modal CAD reconstruction methods on DeepCAD. Here, input modalities are denoted with subscripts: p stands for point clouds, i for images, and t for texts. cadrille trained jointly on point clouds, multi-view images, and texts from the DeepCAD training set (D_{pit}) outperforms the modality-specific baselines. Noticeably, IR is reduced almost twice for point clouds (from 1.1 to 0.4) and 7x for images (3.6 to 0.5).

Training using the large-scale procedurally generated CAD-Recode dataset (R) consistently improves accuracy over training on the DeepCAD dataset. Since we also use a Qwen LLM model as in CAD-Recode (Qwen2-VL-2B against Qwen2-1.5B), comparable quality of point cloud-based reconstruction is expected. When training cadrille on point clouds and images (R_{pi}), it maintains the same accuracy on point clouds but additionally extends to images. After training with point clouds, images, and texts ($S_{pi} + D_i$), cadrille generalizes across modalities without loss of quality on each modality. For fair comparison, we do not apply any RL techniques in this series of experiments, and mix up training datasets trivially for SFT.

Results on Fusion360 and CC3D Both Fusion360 and CC3D datasets do not provide annotations in a compatible format, and are only used for testing in the standard evaluation protocol (Khan et al., 2024a). Accordingly, testing on these datasets is performed in a zero-shot scenario, which allows assessing the generalization ability of CAD reconstruction approaches. Furthermore, since CC3D contains real scans of objects, this experiment emulates real-world application.

We report CAD reconstruction quality from images and point clouds in Tab. 2 and 3, respectively. CADCrafter is the only method performing CAD reconstruction based on multi-view images. However, the authors of CADCrafter only report metrics on the DeepCAD dataset, and benchmarking it on other datasets is problematic since the code has not been released. To establish a baseline in image-based CAD reconstruction, we combine two off-the-shelf state-of-the-art methods, namely, multi-view reconstruction method LRM Hong et al. (2024); Xu et al. (2024a) and CAD-Recode. LRM takes multi-view images as inputs and produces a mesh, which is turned into a point cloud via surface sampling, and this point cloud is then passed to CAD-Recode to create a CAD model. As can be seen in Tab. 2, cadrille trained on CAD-Recode outperforms both baselines.

In Tab. 3, we compare cadrille against the state-of-the-art approaches originally trained on the DeepCAD (CAD-SIGNet) and CAD-Recode datasets. As could be expected, cadrille is on par with CAD-Recode, while delivering substantially better quality w.r.t. CAD-SIGNet.

5.2 REINFORCEMENT LEARNING

RL on single modality boosts other modalities In Tab. 2, we report accuracy of image-based CAD reconstruction on three benchmarks. Respectively, we fine-tune cadrille with images from DeepCAD and Fusion360 datasets. It is worth noticing that while Fusion360 cannot be used

Method	Train	Po	oint Clou	ıd	Multi	-view Ir	nages		Text	
Method	Data	$CD\downarrow$	IoU↑	IR↓	$CD\downarrow$	IoU↑	IR↓	$\mathrm{CD}\!\!\downarrow$	IoU↑	IR↓
PointNet→DeepCAD	D_p	9.64	46.7	7.1						
Point-BERT→HNC-CAD	$\hat{\mathbf{D_p}}$	8.64	65.3	5.6						
MultiCAD	$\hat{D_p}$	8.09		11.5						
TransCAD	$\hat{D_p}$	4.51	65.5	<u>1.1</u>						
PrismCAD	$\mathbf{D}_{\mathbf{p}}^{\mathbf{r}}$	4.28	72.1	16.2						
Point2Cyl	$\hat{\mathbf{D_p}}$	4.27	73.8	3.9						
CAD-Diffuser	$\mathbf{D}_{\mathbf{p}}$	3.02	74.3	1.5						
CAD-SIGNet	D_p	0.29	<u>77.3</u>	5.0						
DINOv2→HNC-CAD	D_i				2.08		10.1			
DINOv2→DeepCAD	D_{i}				1.13		10.6			
CADCrafter	D_i				0.26		3.6			
BERT→DeepCAD	D_t							32.82		10.0
CADmium	D_t							0.38		4.3
Text2CAD	D_t							0.37	<u>71.5</u>	3.7
CAD-Coder	D_t							0.33		5.3
Text-to-CadQuery	D_t							0.22		1.3
cadrille	$\mathrm{D}_{\mathrm{pit}}$	0.25	79.4	0.4	0.25	78.2	0.5	0.21	81.1	<u>1.4</u>
CAD-Recode	R_p	0.18	87.1	3.1						
cadrille	R_{pi}	0.18	87.1	2.1	0.18	86.1	1.5			
cadrille	$R_{pi}+D_t$	0.18	87.1	2.1	0.18	86.1	1.5	0.20	82.1	1.4

Table 1: Results on DeepCAD test set. The best results are **bold**, the second best are <u>underlined</u>. Our cadrille trained jointly on three modalities outperforms all existing modality-specific methods. Here, we report metrics obtained *without* RL fine-tuning or test-time sampling for fair comparison.

Method	RL	Train	Data	Γ	DeepCAI)	F	usion36	0		CC3D	
Method	KL	SFT	RL	$CD\downarrow$	IoU↑	IR↓	$CD\downarrow$	IoU↑	IR↓	$CD\downarrow$	IoU↑	IR↓
LRM→CAD-Recode	Х	R _p	Х	0.53	69.8	14.3	0.62	62.5	18.7	1.19	50.1	20.1
CADCrafter	DPO	$\vec{\mathbf{D_i}}$	D_{i}	0.26		3.6						
cadrille	Х	R_{pi}	X	0.18	86.1	1.5	0.20	77.6	3.2	0.81	56.1	7.7
cadrille	Х	R _{pi} +D _{pi}	Х	0.19	85.6	0.6	0.23	75.2	2.6	1.17	53.1	6.0
cadrille	DPO	R_{pi}	$D_i^- + F_i^-$	0.18	86.9	1.8	0.20	78.5	1.7	0.89	56.0	3.9
cadrille	Dr. CPPO	R_{pi}	$D_i^-+F_i^-$	0.17	92.2	0.0	0.17	84.6	0.0	0.57	65.0	0.1

Table 2: Results of CAD reconstruction from multi-view images. With RL fine-tuning, cadrille achieves best results across three benchmarks.

for direct supervised training, it can still contribute to RL fine-tuning where CAD sequences are not required, so we can benefit from adding it to the mixture. We denote DeepCAD and Fusion360 datasets without CAD sequence annotations as D^- and F^- .

Surprisingly, RL fine-tuning on images appears to be beneficial for other modalities: as reported in Tab. 3, the model tuned on $D_i^- + F_i^-$ (row 6) delivers state-of-the-art quality of CAD reconstruction from point clouds as well.

RL improves metrics in cross-dataset scenario RL fine-tuning with DeepCAD and Fusion360 boosts accuracy on the test splits of the respective datasets. Yet, the performance gain is not limited

Method	RL	Train	Data	D	eepCAI)	F	usion36)	Real-	world C	C3D
Method	KL	SFT	RL	$CD\downarrow$	IoU↑	IR↓	$CD\downarrow$	IoU↑	IR↓	$CD\downarrow$	IoU↑	IR↓
CAD-SIGNet	Х	D_p	Х	0.29	77.3	5.0	0.70	58.4	9.3	4.42	39.1	15.5
CAD-Recode	X	R_p	Х	0.18	87.1	3.1	0.19	79.1	5.0	0.54	60.5	9.8
cadrille	X	R_{pi}	X	0.18	87.1	2.1	0.19	79.8	2.8	0.54	61.8	5.9
cadrille	Х	R _{pi} +D _{pi}	Х	0.19	86.6	0.9	0.22	76.5	2.0	0.79	58.7	4.1
cadrille	DPO	R_{pi}	$D_i^- + F_i^-$	0.18	88.1	0.7	0.19	80.9	1.3	0.54	61.3	2.6
cadrille	Dr. CPPO	R_{pi}	$D_i^- + F_i^-$	0.17	90.2	0.0	0.17	85.0	0.2	0.47	67.9	0.2

Table 3: Results of CAD reconstruction from point clouds. cadrille performs on par with CAD-Recode when trained on the CAD-Recode dataset (R). With RL, cadrille establishes state-of-the-art on DeepCAD, Fusion360 and real-world CC3D.

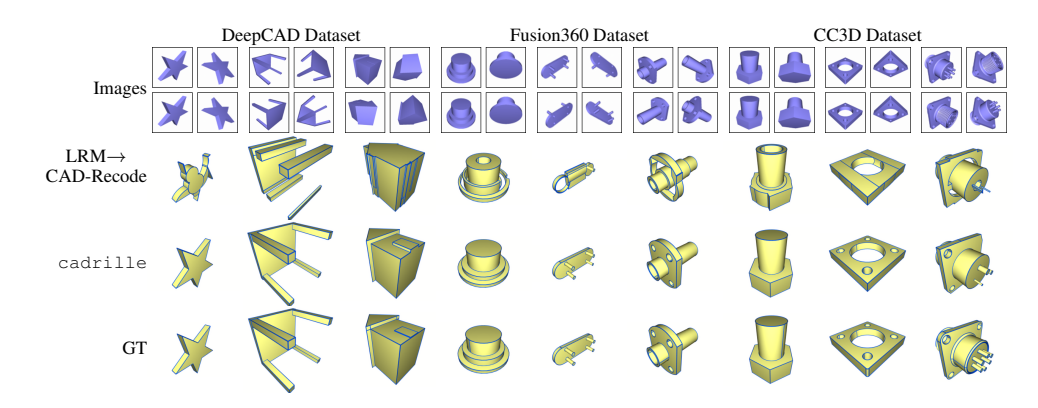


Figure 5: CAD models reconstructed from multi-view images on the DeepCAD, Fusion360, and CC3D datasets.

to the domains seen by a model during SFT and RL fine-tuning. In image-based CAD reconstruction, CD is reduced from 0.81 to 0.57, while IR dropped dramatically from 7.7 to 0.1 (rows 3 and 6, respectively). When testing on point clouds, RL also improves all scores on CC3D, making IR less than 0.2%, which is negligible.

Online RL outperforms offline RL Fine-tuning cadrille using offline DPO reduces IR twice in most cases, while accuracy scores are not affected (rows 3 and 5 in both Tables). In the meantime, Dr. CPPO beats SFT in terms of all metrics, adding 3-9% to IoU scores and bringing IR under 0.2% in all benchmarks (row 6). The observed improvement of CAD reconstruction accuracy aligns well with the experimental results obtained in other tasks where feedback can be programmatically computed Shao et al. (2024).

RL fine-tuning beats SFT on a mixture A common assumption is that mixing datasets improves generalization by increasing data diversity and volume. However, our experiments show that SFT with a plain mixture of CAD-Recode and DeepCAD datasets ($R_{pi}+D_{pi}$, row 4) does not lead to performance gains, and can even degrade results w.r.t. SFT with R_{pi} (row 3). We attribute this effect to the domain gap between datasets, specifically, some CAD operations present in DeepCAD (e.g., symmetric extrusion, extruded cut) are lacking from CAD-Recode.

Qualitative results CAD models obtained with RL fine-tuning are depicted in Fig. 4 (from point clouds) and Fig. 5 (from multi-view images). Compared to predecessors, cadrille produces more geometrically plausible reconstructions and better restores fine details.

6 CONCLUSION

We introduced cadrille, a multimodal CAD reconstruction model that is capable of processing point clouds, multi-view images, and text inputs within a unified VLM-based framework. By adopting a two-stage training paradigm, namely, supervised fine-tuning on synthetic data followed by reinforcement learning fine-tuning with programmatic feedback, we improved both reconstruction quality and validity ratio. Our empirical study demonstrated that online RL approaches are especially beneficial in the CAD reconstruction scenario. cadrille achieves new state-of-theart results in 10 CAD reconstruction benchmarks, including a real-world dataset, highlighting its robustness, generalizability, and potential for further use in applications. Based on our study, we identify the following promising research directions for the future work: 1) combine modalities in one prompt to compensate for low-quality or missing inputs 2) perform RL fine-tuning on point clouds, and 3) increase complexity of procedurally generated data and volume of RL fine-tuning data to better adapt to real-world scans.

REPRODUCIBILITY AND LLM STATEMENT

To ensure reproducibility of our results, we provide implementation details in Appendix D, including Tab. 13 and 14. Additionally, we attach the code performing all training (both SFT and RL) and evaluation procedures reported in this paper, as a supplemental material to the submission. The code will be published upon acceptance. LLMs (namely, ChatGPT) was used only to polish the manuscript.

REFERENCES

- Silvia Ansaldi, Leila De Floriani, and Bianca Falcidieno. Geometric modeling of solid objects by using a face adjacency graph representation. *ACM SIGGRAPH Computer Graphics*, 19(3):131–139, 1985.
- CadQuery Authors. Cadquery/cadquery: Cadquery 2.4.0, January 2024. URL https://doi.org/10.5281/zenodo.10513848.
- Akshay Badagabettu, Sai Sravan Yarlagadda, and Amir Barati Farimani. Query2cad: Generating cad models using natural language queries. *arXiv preprint arXiv:2406.00144*, 2024.
- Antoine Briere-Cote, Louis Rivest, and Roland Maranzana. Comparing 3d cad models: uses, methods, tools and perspectives. *Computer-Aided Design and Applications*, 9(6):771–794, 2012.
- Cheng Chen, Jiacheng Wei, Tianrun Chen, Chi Zhang, Xiaofeng Yang, Shangzhan Zhang, Bingchen Yang, Chuan-Sheng Foo, Guosheng Lin, Qixing Huang, et al. Cadcrafter: Generating computer-aided design models from unconstrained images. In *Proceedings of the IEEE/CVF Conference on Computer Vision and Pattern Recognition*, 2025.
- Tianrun Chen, Chunan Yu, Yuanqi Hu, Jing Li, Tao Xu, Runlong Cao, Lanyun Zhu, Ying Zang, Yong Zhang, Zejian Li, et al. Img2cad: Conditioned 3d cad model generation from single image with structured visual geometry. *arXiv preprint arXiv:2410.03417*, 2024.
- Anna C Doris, Md Ferdous Alam, Amin Heyrani Nobari, and Faez Ahmed. Cad-coder: An open-source vision-language model for computer-aided design code generation. *arXiv* preprint *arXiv*:2505.14646, 2025.
- Tao Du, Jeevana Priya Inala, Yewen Pu, Andrew Spielberg, Adriana Schulz, Daniela Rus, Armando Solar-Lezama, and Wojciech Matusik. Inversecsg: Automatic conversion of 3d models to csg trees. *ACM Transactions on Graphics (TOG)*, 37(6):1–16, 2018.
- Elona Dupont, Kseniya Cherenkova, Dimitrios Mallis, Gleb Gusev, Anis Kacem, and Djamila Aouada. Transcad: A hierarchical transformer for cad sequence inference from point clouds. In *European Conference on Computer Vision*, pp. 19–36. Springer, 2024.
- Kevin Ellis, Maxwell Nye, Yewen Pu, Felix Sosa, Josh Tenenbaum, and Armando Solar-Lezama. Write, execute, assess: Program synthesis with a repl. *Advances in Neural Information Processing Systems*, 32, 2019.
- James D Foley. *Computer graphics: principles and practice*, volume 12110. Addison-Wesley Professional, 1996.
 - Markus Friedrich, Pierre-Alain Fayolle, Thomas Gabor, and Claudia Linnhoff-Popien. Optimizing evolutionary csg tree extraction. In *Proceedings of the Genetic and Evolutionary Computation Conference*, pp. 1183–1191, 2019.
 - Prashant Govindarajan, Davide Baldelli, Jay Pathak, Quentin Fournier, and Sarath Chandar. Cadmium: Fine-tuning code language models for text-driven sequential cad design. *arXiv* preprint *arXiv*:2507.09792, 2025.
 - Yandong Guan, Xilin Wang, Xingxi Ming, Jing Zhang, Dong Xu, and Qian Yu. Cad-coder: Text-to-cad generation with chain-of-thought and geometric reward. *arXiv preprint arXiv:2505.19713*, 2025.

- Haoxiang Guo, Shilin Liu, Hao Pan, Yang Liu, Xin Tong, and Baining Guo. Complexgen: Cad reconstruction by b-rep chain complex generation. *ACM Transactions on Graphics (TOG)*, 41(4): 1–18, 2022.
- Changqi He, Shuhan Zhang, Liguo Zhang, and Jiajun Miao. Cad-coder: Text-guided cad files code generation. *arXiv preprint arXiv:2505.08686*, 2025.
 - Yicong Hong, Kai Zhang, Jiuxiang Gu, Sai Bi, Yang Zhou, Difan Liu, Feng Liu, Kalyan Sunkavalli, Trung Bui, and Hao Tan. Lrm: Large reconstruction model for single image to 3d. In *International Conference on Learning Representations*, 2024.
 - Pradeep Kumar Jayaraman, Joseph G Lambourne, Nishkrit Desai, Karl DD Willis, Aditya Sanghi, and Nigel JW Morris. Solidgen: An autoregressive model for direct b-rep synthesis. *Transactions on Machine Learning Research*, 2023.
 - Kacper Kania, Maciej Zieba, and Tomasz Kajdanowicz. Ucsg-net-unsupervised discovering of constructive solid geometry tree. *Advances in neural information processing systems*, 33:8776–8786, 2020.
 - Mohammad Sadil Khan, Elona Dupont, Sk Aziz Ali, Kseniya Cherenkova, Anis Kacem, and Djamila Aouada. Cad-signet: Cad language inference from point clouds using layer-wise sketch instance guided attention. In *Proceedings of the IEEE/CVF Conference on Computer Vision and Pattern Recognition*, pp. 4713–4722, 2024a.
 - Mohammad Sadil Khan, Sankalp Sinha, Talha Uddin, Didier Stricker, Sk Aziz Ali, and Muhammad Zeshan Afzal. Text2cad: Generating sequential cad designs from beginner-to-expert level text prompts. *Advances in Neural Information Processing Systems*, 37:7552–7579, 2024b.
 - Joseph G Lambourne, Karl DD Willis, Pradeep Kumar Jayaraman, Aditya Sanghi, Peter Meltzer, and Hooman Shayani. Brepnet: A topological message passing system for solid models. In *Proceedings of the IEEE/CVF conference on computer vision and pattern recognition*, pp. 12773–12782, 2021.
 - Joseph George Lambourne, Karl Willis, Pradeep Kumar Jayaraman, Longfei Zhang, Aditya Sanghi, and Kamal Rahimi Malekshan. Reconstructing editable prismatic cad from rounded voxel models. In *SIGGRAPH Asia 2022 Conference Papers*, pp. 1–9, 2022.
 - Jiahao Li, Weijian Ma, Xueyang Li, Yunzhong Lou, Guichun Zhou, and Xiangdong Zhou. Cadlama: leveraging large language models for computer-aided design parametric 3d model generation. In *Proceedings of the Computer Vision and Pattern Recognition Conference*, pp. 18563–18573, 2025a.
 - Yuan Li, Cheng Lin, Yuan Liu, Xiaoxiao Long, Chenxu Zhang, Ningna Wang, Xin Li, Wenping Wang, and Xiaohu Guo. Caddreamer: Cad object generation from single-view images. In *Proceedings of the IEEE/CVF International Conference on Computer Vision*, 2025b.
 - Zhihang Lin, Mingbao Lin, Yuan Xie, and Rongrong Ji. Cppo: Accelerating the training of group relative policy optimization-based reasoning models. *arXiv preprint arXiv:2503.22342*, 2025.
 - Mingjie Liu, Shizhe Diao, Ximing Lu, Jian Hu, Xin Dong, Yejin Choi, Jan Kautz, and Yi Dong. Prorl: Prolonged reinforcement learning expands reasoning boundaries in large language models. *arXiv preprint arXiv:2505.24864*, 2025a.
 - Yilin Liu, Jiale Chen, Shanshan Pan, Daniel Cohen-Or, Hao Zhang, and Hui Huang. Split-and-fit: Learning b-reps via structure-aware voronoi partitioning. *ACM Transactions on Graphics (TOG)*, 43(4):1–13, 2024a.
 - Yujia Liu, Anton Obukhov, Jan Dirk Wegner, and Konrad Schindler. Point2cad: Reverse engineering cad models from 3d point clouds. In *Proceedings of the IEEE/CVF Conference on Computer Vision and Pattern Recognition*, pp. 3763–3772, 2024b.
 - Zichen Liu, Changyu Chen, Wenjun Li, Penghui Qi, Tianyu Pang, Chao Du, Wee Sun Lee, and Min Lin. Understanding r1-zero-like training: A critical perspective. *arXiv* preprint *arXiv*:2503.20783, 2025b.

- Weijian Ma, Shuaiqi Chen, Yunzhong Lou, Xueyang Li, and Xiangdong Zhou. Draw step by step:
 Reconstructing cad construction sequences from point clouds via multimodal diffusion. In *Proceedings of the IEEE/CVF Conference on Computer Vision and Pattern Recognition*, pp. 27154–27163, 2024.
 - Dimitrios Mallis, Ali Sk Aziz, Elona Dupont, Kseniya Cherenkova, Ahmet Serdar Karadeniz, Mohammad Sadil Khan, Anis Kacem, Gleb Gusev, and Djamila Aouada. Sharp challenge 2023: Solving cad history and parameters recovery from point clouds and 3d scans. overview, datasets, metrics, and baselines. In *Proceedings of the IEEE/CVF International Conference on Computer Vision*, pp. 1786–1795, 2023.
 - Dimitrios Mallis, Ahmet Serdar Karadeniz, Sebastian Cavada, Danila Rukhovich, Niki Foteinopoulou, Kseniya Cherenkova, Anis Kacem, and Djamila Aouada. Cad-assistant: Toolaugmented vllms as generic cad task solvers? arXiv preprint arXiv:2412.13810, 2024.
 - Chandrakana Nandi, James R Wilcox, Pavel Panchekha, Taylor Blau, Dan Grossman, and Zachary Tatlock. Functional programming for compiling and decompiling computer-aided design. *Proceedings of the ACM on Programming Languages*, 2(ICFP):1–31, 2018.
 - Rafael Rafailov, Archit Sharma, Eric Mitchell, Christopher D Manning, Stefano Ermon, and Chelsea Finn. Direct preference optimization: Your language model is secretly a reward model. *Advances in Neural Information Processing Systems*, 36:53728–53741, 2023.
 - Daxuan Ren, Jianmin Zheng, Jianfei Cai, Jiatong Li, Haiyong Jiang, Zhongang Cai, Junzhe Zhang, Liang Pan, Mingyuan Zhang, Haiyu Zhao, et al. Csg-stump: A learning friendly csg-like representation for interpretable shape parsing. In *Proceedings of the IEEE/CVF international conference on computer vision*, pp. 12478–12487, 2021.
 - Daxuan Ren, Jianmin Zheng, Jianfei Cai, Jiatong Li, and Junzhe Zhang. Extrudenet: Unsupervised inverse sketch-and-extrude for shape parsing. In *European Conference on Computer Vision*, pp. 482–498. Springer, 2022.
 - Danila Rukhovich, Elona Dupont, Dimitrios Mallis, Kseniya Cherenkova, Anis Kacem, and Djamila Aouada. Cad-recode: Reverse engineering cad code from point clouds. *arXiv preprint arXiv:2412.14042*, 2024.
 - John Schulman, Filip Wolski, Prafulla Dhariwal, Alec Radford, and Oleg Klimov. Proximal policy optimization algorithms. *arXiv preprint arXiv:1707.06347*, 2017.
 - Zhihong Shao, Peiyi Wang, Qihao Zhu, Runxin Xu, Junxiao Song, Xiao Bi, Haowei Zhang, Mingchuan Zhang, YK Li, Y Wu, et al. Deepseekmath: Pushing the limits of mathematical reasoning in open language models. *arXiv preprint arXiv:2402.03300*, 2024.
 - Gopal Sharma, Rishabh Goyal, Difan Liu, Evangelos Kalogerakis, and Subhransu Maji. Csgnet: Neural shape parser for constructive solid geometry. In *Proceedings of the IEEE Conference on Computer Vision and Pattern Recognition*, pp. 5515–5523, 2018.
 - Gopal Sharma, Difan Liu, Subhransu Maji, Evangelos Kalogerakis, Siddhartha Chaudhuri, and Radomír Měch. Parsenet: A parametric surface fitting network for 3d point clouds. In *Computer Vision–ECCV 2020: 16th European Conference, Glasgow, UK, August 23–28, 2020, Proceedings, Part VII 16*, pp. 261–276. Springer, 2020.
 - Yonglong Tian, Andrew Luo, Xingyuan Sun, Kevin Ellis, William T. Freeman, Joshua B. Tenenbaum, and Jiajun Wu. Learning to infer and execute 3d shape programs. In *International Conference on Learning Representations*, 2019.
 - Kehan Wang, Jia Zheng, and Zihan Zhou. Neural face identification in a 2d wireframe projection of a manifold object. In *Proceedings of the IEEE/CVF Conference on Computer Vision and Pattern Recognition*, pp. 1622–1631, 2022.
 - Peng Wang, Shuai Bai, Sinan Tan, Shijie Wang, Zhihao Fan, Jinze Bai, Keqin Chen, Xuejing Liu, Jialin Wang, Wenbin Ge, et al. Qwen2-vl: Enhancing vision-language model's perception of the world at any resolution. *arXiv preprint arXiv:2409.12191*, 2024.

- Ruiyu Wang, Yu Yuan, Shizhao Sun, and Jiang Bian. Text-to-cad generation through infusing visual feedback in large language models. *arXiv preprint arXiv:2501.19054*, 2025a.
- Siyu Wang, Cailian Chen, Xinyi Le, Qimin Xu, Lei Xu, Yanzhou Zhang, and Jie Yang. Cadgpt: Synthesising cad construction sequence with spatial reasoning-enhanced multimodal llms. In *Proceedings of the AAAI Conference on Artificial Intelligence*, volume 39, pp. 7880–7888, 2025b.
- Xiaogang Wang, Yuelang Xu, Kai Xu, Andrea Tagliasacchi, Bin Zhou, Ali Mahdavi-Amiri, and Hao Zhang. Pie-net: Parametric inference of point cloud edges. *Advances in neural information processing systems*, 33:20167–20178, 2020.
- Xilin Wang, Jia Zheng, Yuanchao Hu, Hao Zhu, Qian Yu, and Zihan Zhou. From 2d cad drawings to 3d parametric models: A vision-language approach. In *Proceedings of the AAAI Conference on Artificial Intelligence*, volume 39, pp. 7961–7969, 2025c.
- Karl DD Willis, Yewen Pu, Jieliang Luo, Hang Chu, Tao Du, Joseph G Lambourne, Armando Solar-Lezama, and Wojciech Matusik. Fusion 360 gallery: A dataset and environment for programmatic cad construction from human design sequences. *ACM Transactions on Graphics (TOG)*, 40(4): 1–24, 2021.
- Rundi Wu, Chang Xiao, and Changxi Zheng. Deepcad: A deep generative network for computer-aided design models. In *Proceedings of the IEEE/CVF International Conference on Computer Vision*, pp. 6772–6782, 2021.
- Haoyang Xie and Feng Ju. Text-to-cadquery: A new paradigm for cad generation with scalable large model capabilities. *arXiv preprint arXiv:2505.06507*, 2025.
- Jiale Xu, Weihao Cheng, Yiming Gao, Xintao Wang, Shenghua Gao, and Ying Shan. Instantmesh: Efficient 3d mesh generation from a single image with sparse-view large reconstruction models. *arXiv preprint arXiv:2404.07191*, 2024a.
- Jingwei Xu, Chenyu Wang, Zibo Zhao, Wen Liu, Yi Ma, and Shenghua Gao. Cad-mllm: Unifying multimodality-conditioned cad generation with mllm. *arXiv preprint arXiv:2411.04954*, 2024b.
- Xiang Xu, Karl DD Willis, Joseph G Lambourne, Chin-Yi Cheng, Pradeep Kumar Jayaraman, and Yasutaka Furukawa. Skexgen: Autoregressive generation of cad construction sequences with disentangled codebooks. In *International Conference on Machine Learning*, pp. 24698–24724. PMLR, 2022.
- Xiang Xu, Pradeep Kumar Jayaraman, Joseph G Lambourne, Karl DD Willis, and Yasutaka Furukawa. Hierarchical neural coding for controllable cad model generation. In *International Conference on Machine Learning*, pp. 38443–38461, 2023.
- Xiang Xu, Joseph Lambourne, Pradeep Jayaraman, Zhengqing Wang, Karl Willis, and Yasutaka Furukawa. Brepgen: A b-rep generative diffusion model with structured latent geometry. *ACM Transactions on Graphics (TOG)*, 43(4):1–14, 2024c.
- Xiaolong Yin, Xingyu Lu, Jiahang Shen, Jingzhe Ni, Hailong Li, Ruofeng Tong, Min Tang, and Peng Du. Rlcad: Reinforcement learning training gym for revolution involved cad command sequence generation. *arXiv preprint arXiv:2503.18549*, 2025.
- Fenggen Yu, Zhiqin Chen, Manyi Li, Aditya Sanghi, Hooman Shayani, Ali Mahdavi-Amiri, and Hao Zhang. Capri-net: Learning compact cad shapes with adaptive primitive assembly. In *Proceedings* of the IEEE/CVF conference on computer vision and pattern recognition, pp. 11768–11778, 2022.
- Fenggen Yu, Qimin Chen, Maham Tanveer, Ali Mahdavi Amiri, and Hao Zhang. D2csg: Unsupervised learning of compact csg trees with dual complements and dropouts. *Advances in Neural Information Processing Systems*, 36:22807–22819, 2023.
- Yu Yuan, Shizhao Sun, Qi Liu, and Jiang Bian. Cad-editor: A locate-then-infill framework with automated training data synthesis for text-based cad editing. *arXiv preprint arXiv:2502.03997*, 2025.

Yang Yue, Zhiqi Chen, Rui Lu, Andrew Zhao, Zhaokai Wang, Shiji Song, and Gao Huang. Does reinforcement learning really incentivize reasoning capacity in llms beyond the base model? *arXiv* preprint arXiv:2504.13837, 2025.

Chao Zhang, Arnaud Polette, Romain PINQUIÉ, Mirai Iida, Henri De Charnace, and Jean-Philippe Pernot. Reinforcement learning-based parametric cad models reconstruction from 2d orthographic drawings. *Available at SSRN 5174280*, 2025a.

Zhanwei Zhang, Shizhao Sun, Wenxiao Wang, Deng Cai, and Jiang Bian. Flexcad: Unified and versatile controllable cad generation with fine-tuned large language models. *International Conference on Learning Representations*, 2025b.

A QUALITATIVE RESULTS

Text-based CAD reconstruction Fig. 6 shows results of text-based CAD reconstruction on the DeepCAD dataset. Long textual descriptions still cannot define even simple 3D shapes comprehensively and unambiguously, making CAD reconstruction from textual inputs the most challenging. Both Text2CAD and cadrille struggle to recover correct geometry, yet our approach yields more accurate predictions, which is also reflected in the quantitative metrics.

Real-world single-image experiment Since our cadrille is trained only on synthetic renders, sim-to-real transfer can be eligibly questioned. To address the potential concerns about the applicability of our approach, apart from validating on real scans from the CC3D dataset, we also experiment with CAD reconstruction from a single real-world image.

The pipeline consists of three steps. First, an input image is processed using the recent image-to-mesh InstantMesh Xu et al. (2024a) method, that produces a mesh. Second, we follow the same protocol as in other experiments to convert this mesh to a point cloud 7 or four multi-view images 8. We claim that the obtained results look promising, and this practical pipeline opens new opportunities of in-the-wild CAD reconstruction.

Failure cases are depicted in Fig. 9. cadrille always predicts a geometrically relevant shape, but still might miss details, especially for objects with complex and granular surfaces.

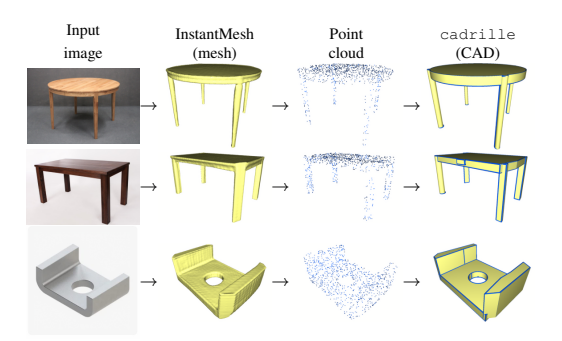


Figure 7: Results of CAD reconstruction from a *single* real-world image. cadrille takes point clouds sampled from mesh reconstructed by InstantMesh as input.

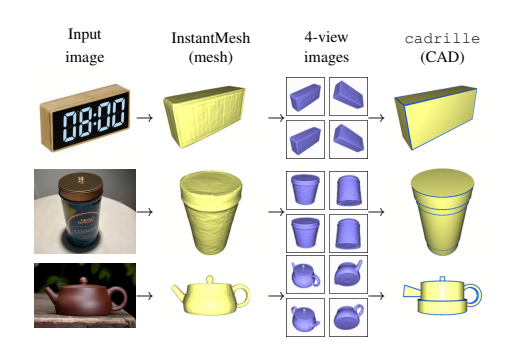


Figure 8: Results of CAD reconstruction from a *single* real-world image. cadrille takes multi-view images rendered from mesh reconstructed by InstantMesh as input.

B QUANTITATIVE RESULTS

Results on Omni-CAD Omni-CAD is claimed to be the first multimodal dataset featuring point clouds, multi-view images, and textual descriptions of CAD models. However, texts are not fully utilized for CAD reconstruction, since generated models are only assessed in a user study and no standard quantitative metrics are provided (Xu et al., 2024b). Accordingly, we validate cadrille only in point cloud-based and image-based scenarios, and report the evaluation results in Tab. 4.

756 Text Text2CAD cadrille GT

Create a new coordinate system with Euler angles set to 0 degrees for the first 2 angles and -90 degrees for the third angle. Set the translation vector to 0.2766, 0.1476, and 0.2766. On the first face, draw a 2-dimensional sketch consisting of 2 loops. For the first loop, draw a circle with its center at 0.0984, 0.0984, and a radius of 0.0984. For the second loop, draw another circle with the same center but a smaller radius of 0.048. Scale the entire 2-dimensional sketch by a factor of 0.1969. Rotate and translate the scaled 2-dimensional sketch using the previously defined coordinate system settings. Extrude the outer loop (the larger circle) by 0.1476 units in the direction opposite to the normal. Similarly, extrude the inner loop (the smaller circle) by the same distance in the same direction. Ensure that the extrusion results in a new solid body. The final dimensions of the cylindrical object with a hole should be a length of 0.1969 units, a width of 0.1969 units, and a height of 0.1476 units. The object resembles a doughnut shape, with a smooth surface and a uniform diameter.



Create a new coordinate system with Euler Angles set to [0, 0, 0] and a Translation Vector of [0, 0, 0]. Draw a 2D sketch on the XY plane and define the first face using a loop of 4 lines. The first line starts at (0, 0) and ends at (0.5, 0). The second line starts at (0.5, 0) and ends at (0.5, 0.75). The third line starts at (0.5, 0.75) and ends at (0, 0, 0.75). The fourth line starts at (0, 0.75) and ends at (0, 0). Scale the 2D sketch using a scale factor of 0.75. Transform the scaled 2D sketch into 3D using the same Euler Angles and Translation Vector. Extrude the 2D sketch to create a 3D model with an extrusion depth of 0.5 units towards the normal. Create a new solid body with this extrusion and verify the dimensions: length of 0.5 units, width of 0.75 units, and height of 0.5 units.

Next, create a new coordinate system with Euler Angles set to [0, 0, 0] and a Translation Vector of [0.1, 0, 0.5]. Draw a 2D sketch on the XY plane and define the first face using a loop of 4 lines. The first line starts at (0, 0) and ends at (0.3, 0.75). The second line starts at (0.3, 0) and ends at (0.3, 0.75). The fourth line starts at (0, 0.75) and ends at (0, 0.) Scale the 2D sketch using a scale factor of 0.75. Transform the scaled 2D sketch into 3D using the same Euler Angles and Translation Vector. Extrude the 2D sketch to create a 3D model with an extrusion depth of 0.4 units in the opposite direction of the normal. Remove material from the existing body using this extrusion and verify the dimensions: length of 0.3 units, width of 0.75 units, and height of 0.4 units.

The final shape is a U-shaped bracket with a rectangular cross-section. It has 2 parallel sides and an open space in the middle. The dimensions are: length of 0.5 units, width of 0.75 units, and height of 0.5 units.

Create a new coordinate system with Euler angles set to 0, 0, and -90 degrees, and a translation vector of 0, 0.2812, and 0.1406. On the first face, draw the first loop as a rectangle with the following lines: the first line starts at (0, 0) and ends at (0.3398, 0); the second line starts at (0.3398, 0) and ends at (0.3398, 0.4687); the third line starts at (0.3398, 0.4687) and ends at (0, 0.4687); the fourth line starts at (0, 0.4687) and ends at (0, 0). In the second loop, draw a circle with a center at (0.2344, 0.3344) and a radius of 0.0937. In the third loop, draw a circle with a center at (0.2344, 0.3867) and a radius of 0.0176. In the fourth loop, draw a circle with a center at (0.2344, 0.3867) and a radius of 0.0176. Apply a scale factor of 0.4687 to the entire sketch. Rotate the scaled sketch using the Euler angles set in the coordinate system and translate it using the translation vector. Extrude the sketch 0.2812 units along the normal direction without extruding in the opposite direction to create a new solid body. The final dimensions of the rectangular box with circular cutouts are a length of 0.3398 units, a width of 0.4687 units, and a height of 0.2812 units.



Figure 6: Results of text-based CAD reconstruction on the DeepCAD dataset.

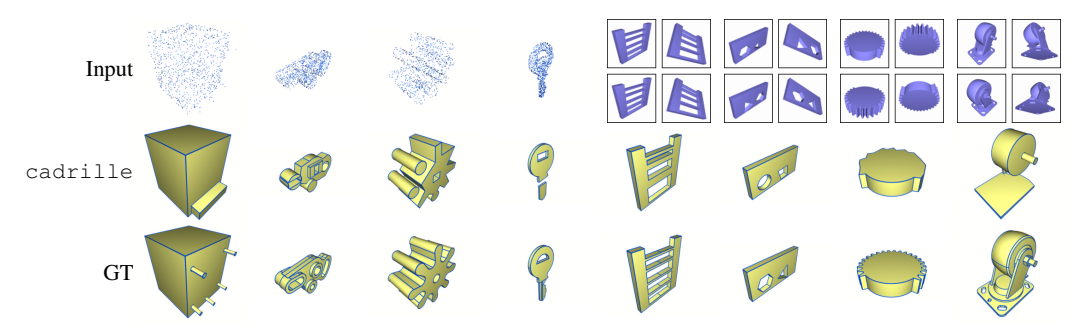


Figure 9: Failure cases of CAD reconstruction from point clouds and multi-view images on Deep-CAD, Fusion360, and CC3D datasets.

Method	RL	Po	oint Clou	ıd	Multi	-view In	nages
Method	KL	$CD\downarrow$	IoU↑	IR↓	$CD\downarrow$	IoU↑	ĬR↓
DeepCAD	Х	45.1		5.7			
CAD-MLLM	X	18.5		1.3	37.7		
Point2CAD	X	12.5		11.4			
cadrille	X	1.00	79.1	3.7	1.22	77.0	6.2
cadrille	✓	0.77	84.2	0.6	0.60	84.8	0.0

Table 4: Results of CAD reconstruction from point clouds and multi-view images from the Omni-CAD dataset. We specify *mean* CD since it is the only CD metric reported by CAD-MLLM.

Method	Train	CD↓	IoU↑	IR↓
DeepCAD	Dp	89.2	39.9	25.2
MultiCAD	D_p	42.2		16.5
HNC-CAD	$\hat{\mathbf{D_p}}$	36.8	63.5	7.3
TransCAD	$\hat{\mathbf{D_p}}$	33.4	60.2	2.4
CAD-Diffuser	$\hat{D_p}$	3.85	63.2	1.7
CAD-SIGNet	$\hat{\mathbf{D_p}}$	0.70	58.3	9.3
cadrille	$\hat{\mathbf{D_p}}$	0.66	63.7	0.6
CAD-Recode	Rp	0.19	79.1	5.0
cadrille	$\hat{R_p}$	0.19	79.8	2.8

Table 5: Results of point-based CAD reconstruction on the Fusion360 test set. All reported metrics are obtained using an SFT model without RL.

The metrics of prior works are cited in accordance to CAD-MLLM, respectively, we include Point2CAD (Liu et al., 2024b), which is the only non-CAD-sequence method producing B-Reps in our evaluation. Moreover, we multiply their values by 10 for consistency with our format, since they report all scores at 10^2 scale, while we use 10^3 scale in all tables. In general, the results on Omni-CAD are similar to the ones obtained in other benchmarks, namely, cadrille achieves the highest IoU score among all tested approaches, while IR is the lowest with the large margin, reaching 0.0 in image-based benchmark due to RL fine-tuning.

More baselines on Fusion360 In Tab. 5, we compare cadrille to more point cloud-based CAD reconstruction baselines on the Fusion360 dataset. As can be observed, cadrille outperforms competitors trained either on DeepCAD or CAD-Recode datasets. The only existing three-modal approach CAD-MLLM reports only mean CD for the Fusion360 dataset, so we list it among other approaches in another Tab. 6. As can be observed, CAD-MLLM far behind our method, with mean CD value being two orders of magnitude larger than of cadrille.

Mean CD Mean CD is sometimes reported alongside *median* CD. In the main paper, we only provided median CD as the most common CAD reconstruction metric. Nevertheless, the evaluation protocol might be considered incomplete without mean CD. In Tab. 6, we report *mean* CD metric for all scenarios on all three datasets. Our SFT model outperforms all competitors. The gain is especially tangible in text-based CAD reconstruction, where Text2CAD mean CD is reduced 6x from 26.4 to 3.95. With RL fine-tuning (Dr. CPPO) the new state-of-the-art is set in both image-based and point cloud-based CAD reconstruction on all three datasets. The most dramatic improvement is demonstrated on the Fusion360 dataset, where the relative increase exceeds 40% (Tab. 5).

Method	Train	RL	I	DeepCAD		Fusi	on360	CC	C3D
Method	Data	KL	Points	Images	Text	Points	Images	Points	Images
PointNet→DeepCAD	D_p	×	42.5			76.1			
CAD-MLLM	O_{pit}	×				33.9			
CAD-SIGNet	$\hat{\mathbf{D_p}}$	×	6.81			14.5		32.6	
CAD-Recode	R_p	X	0.83			1.21		3.21	
LRM→CAD-Recode	R_p	×		3.36			4.33		4.75
BERT→DeepCAD	$\hat{\mathbf{D_t}}$	×			97.9				
CAD-Coder	D_t	X			74.6				
Text2CAD	D_t	X			26.4				
Text-to-CadQuery	D_t	×			11.8				
cadrille	D_{pit}	X	3.43	3.57	4.24	7.61	8.59	12.2	13.2
cadrille	$R_{pi}+D_t$	Х	0.76	0.81	3.95	1.10	1.13	2.32	3.50
CADFusion	D_t	DPO			19.9				
CAD-Coder	D_t	GRPO			6.54				
cadrille	R_{pi}	DPO	0.61	1.35		0.84	1.27	2.32	3.33
cadrille	R_{pi}	Dr. CPPO	0.57	0.43		0.58	0.64	1.86	2.68

Table 6: *Mean* CD scores obtained across all benchmarks and available input modalities. RL fine-tuning is performed using $D_i^-+F_i^-$ data.

Method	$\mathrm{CD}{\downarrow}$	IoU↑	$IR\downarrow$
GPT-40	62.6		64.4
CAD-GPT	9.77		1.6
DINOv2→HNC-CAD	2.14		11.4
Img2CAD	1.60		28.8
DINOv2→DeepCAD	1.26		12.3
CADCrafter	0.72		8.1
cadrille	0.21	81.7	1.3

Table 7: Results of CAD reconstruction from a *sin-gle* image on the DeepCAD dataset. All reported metrics are obtained with an SFT model without RL.

Method	CD↓	IoU↑	IR↓
GPT-o4-mini cadrille	2.37	60.4	15.9
	0.17	92.2	0.0

Table 8: Results of CAD reconstruction from multi-view images on the Deep-CAD dataset.

 Single-image CAD reconstruction To compare against single-image CAD reconstruction methods, namely, CAD-GPT (Wang et al., 2025b) and Img2CAD (Chen et al., 2024), we conduct an experiment with single-view images on the DeepCAD test set. Our SFT model improves over CAD-Crafter (Chen et al., 2025), reducing median CD from 0.72 to 0.21. As could be expected, the results of single-view CAD reconstruction are slightly inferior to the ones obtained from multi-view images (81% vs 86% IoU).

Zero-shot CAD reconstruction Image-based CAD reconstruction can be performed in zero-shot way using existing VLMs. CAD-GPT sets a weak baseline using GPT-40, that has an invalidity ratio of 64% Tab. 7

We construct another baseline for CAD reconstruction from multi-view images. Four images rendered with orthogonal viewing directions are given to GPT-o4-mini to produce a Python code of CAD model. We apply iterative closest point (ICP) to align predictions before computing metrics so that correct predictions with wrong orientation are not penalized. As can be seen in Tab. 8, this strategy allows achieving significantly better results compared to CAD-GPT. Still, invalidity ratio is as high as 15% and IoU is 30% lower compared to our cadrille.

Inference time When target at practical use, efficiency is an issue. In Tab. 9, we compare inference time of our multimodal cadrille against previous best single-modal methods: CAD-Recode, Text2CAD, and our baseline LRM→CAD-Recode.

Our cadrille is built on top of Qwen2-VL-2B, the smallest Qwen2 model with vision capabilities. When inferred on point clouds, it is 20% slower than CAD-Recode using Qwen2-1.5B. The image inference takes comparable time to proceed. Processing text prompts from Text2CAD dataset lasts notably longer, so that the inference time almost doubles and reaches 3.9 seconds. Text2CAD uses a smaller and faster BERT-large model, that allows achieving efficiency at cost of accuracy. Compared to Text2CAD, cadrille delivers 6x better mean CD 6 being only 2x slower.

C ABLATION EXPERIMENTS

RL fine-tuning vs test-time sampling? A natural concern about the RL fine-tuning is that it might compromise the diversity of responses, hence affecting the final prediction quality. To address this, we conduct an ablation study to investigate how the number of test-time samples affects the performance of both CAD-Recode and cadrille. As reported in 11, CAD-Recode produces more accurate results with an increasing number of samples, but remains inferior to cadrille. In all the benchmarks, cadrille with 1 sample consistently outperforms CAD-Recode with 2 samples in both accuracy and invalidity ratio. In terms of IR, cadrille with 1 sample is better than CAD-Recode with as many as 10 samples, which actually proves RL to boost the robustness of the model.

As could be expected, the gap between IoU@1 with and without RL being significantly larger than the gap between IoU@k (e.g. k=10) with and without RL. This result aligns perfectly with the recent evidence coming from the math domain (see Fig. 2 of Yue et al. (2025) and Fig. 4 of Liu et al. (2025a)).

Method	LLM	Points	Images	Text
CAD-Recode	Qwen2-1.5B	1.8		
LRM→CAD-Recode	Qwen2-1.5B		4.4	
Text2CAD	BERT-336M			1.7
cadrille	Qwen2-VL-2B	2.0	2.0	3.9

Table 9: Inference time in seconds measured on the DeepCAD dataset. All methods are benchmarked on the single H100 GPU with a batch size of 1.

K	DeepCAD	Fusion360	CC3D
2	77.3	70.0	49.7
3	86.2	77.8	55.6
5	86.9	78.5	56.0

Table 10: Results of image-based CAD reconstruction on three datasets, obtained with varying number of samples K in DPO. IoU scores are reported.

			Deep	CAD					Fusio	n360					CC	3D		
# samples	1		2		10)	1	1 2 10)	1		2		10			
	IoU↑	IR↓	IoU↑	IR↓	IoU↑	IR↓	IoU↑	IR↓	IoU↑	IR↓	IoU↑	IR↓	IoU↑	IR	IoU↑	IR↓	IoU↑	IR↓
CAD-Recode	87.1	3.1	89.9	0.9	92.0	0.4	79.1	5.0	83.6	1.3	87.8	0.5	60.5	9.8	64.5	1.7	74.2	0.3
cadrille	90.2	0.0	91.6	0.0	93.1	0.0	85.0	0.2	86.8	0.1	89.1	0.0	67.9	0.2	70.9	0.2	74.7	0.1

Table 11: Results of point-based CAD reconstruction with test-time sampling.

	RL 1	D	eepCAI)	F	Fusion360 CC3D			CC3D		
R_{th}	DeepCAD	Fusion360	$CD\downarrow$	IoU↑	IR↓	$CD\downarrow$	IoU↑	IR↓	$CD\downarrow$	IoU↑	IR↓
1	10k	0.7k	0.18	89.0	1.0	0.18	81.0	2.6	0.74	59.8	6.3
3	20k	1.4k	0.17	90.4	0.7	0.18	82.3	0.9	0.63	62.4	4.0
5	30k	2k	0.17	90.9	0.2	0.17	83.5	0.5	0.62	62.3	0.9
6.2	40k	2.5k	0.17	91.2	0.1	0.17	83.9	0.2	0.60	63.3	0.7
7.5	50k	3k	0.17	92.2	0.0	0.17	84.6	0.0	0.57	65.0	0.1

Table 12: Results of CAD reconstruction from multi-view images with varying amount of data used for RL fine-tuning.

Data for RL fine-tuning As described in Sec. 4.4 in the main paper, not all available data is used for RL fine-tuning, but only the most hard examples are considered. By varying the hard-mining threshold $R_{\rm th}$, we control the difficulty level and the ratio of data selected for fine-tuning. Finding the proper balance is crucial for RL fine-tuning, since it has a notably larger time- and memory footprint compared to SFT, and is hardly feasible without hard example mining.

In Tab. 12, we report results obtained when fine-tuned on data of different volume. All metrics improve gradually with an increase of the amount of the training data. Still, all results reported in this table supersede the SFT baseline (Tab. 2 of the main paper).

Number of samples in DPO We investigate how the number of samples used for RL fine-tuning affects the final results. In Tab. 10, we report IoU scores for image-based reconstruction on all three datasets after 20 epochs of DPO fine-tuning. Performance is unstable with only K=2 samples, while our default value of K=5 yields the best performance. The difference between K=3 and K=5 is less than 1% of IoU, suggesting that the model saturates with few samples, so 5 samples are sufficient.

D IMPLEMENTATION DETAILS

Architecture Our model is built on top of Qwen2-VL Wang et al. (2024) and uses its native capabilities of image and text understanding. In all experiments on multi-view image CAD reconstruction, we use four images. Images are rendered with fixed camera positions, and concatenated into 2x2 grid, forming a combined image of size 268×268 px (as shown in Fig. 8 and 9). This combined image is passed through the Qwen vision encoder, that outputs 400 input tokens. The point cloud injecting into LLM is implemented exactly as in CAD-Recode. Specifically, our input consists of 256 unordered 3D points without normals, sampled from the surface using the furthest point sampling method. The points are projected into shared embedding space with a single linear layer.

Training SFT in cadrille mostly follows the training procedure of CAD-Recode. The only difference is using batch size of 8 and four gradient accumulation steps due to increase of memory for longer prompts in the multimodal scenario. The SFT model is trained with AdamW optimizer for 120k steps and learning rate of 2e-4 on a single H100 GPU.

RL fine-tuning The RL fine-tuning hyperparameters are listed in Tab. 13 (DPO) and 14 (Dr. CPPO). In each experiment, the model is initialized with the weights of an SFT model trained on point clouds and images, and then fine-tuned only on images. All fine-tuning experiments are performed on 8 H100 GPUs.

Value
Adam
20
160
1e-05
0.3
5

Table 13.	DPO t	uning	hyperparameters.
Table 15.	リトワモ	umme	nvberbarameters.

Hyperparameter	Value
Optimizer	Adam
Number of epochs	20
Batch size	128
Learning rate	3e-05
Updates per batch	3
PPO ϵ	0.1
GRPO group size (G)	16
CPPO number of samples (N)	4

Table 14: RL fine-tuning hyperparameters.

E MISCELLANEOUS

Python codes In Fig. 10, we provide Python code with CadQuery library, produced by cadrille. When executed, these Python scripts generate CAD models. Evidently, cadrille is not limited to basic geometric primitives from the DeepCAD dataset (such as line, arc, circle), but is also capable of producing more advanced shapes from the CAD-Recode dataset (box, rectangle, cylinder).

CC3D scans Following CAD-Recode, we treat experiments with CC3D dataset as an emulation of a real-world experiment. CC3D contains scans of the physical objects paired with ground truth CAD models. As shown in Fig. 11, CC3D scans contain artifacts such as surface noise, smoothed edges, and missing parts. In our experiments, we sample points from the surfaces of these real noisy scans instead of the perfect CAD models, which essentially makes the experimental scenario much more realistic.

```
X
```

```
import cadquery as cq
w0=cq.Workplane('XY',origin=(0,0,11))
r=w0.sketch().segment((-100,23),(-43,-23)).segment((-63,-95)).segment((0,-55))
    .segment((62,-96)).segment((42,-23)).segment((100,23)).segment((27,26))
    .segment((0,96)).segment((-26,26)).close().assemble().finalize().extrude(-23)
```



```
import cadquery as cq
w0=cq.Workplane('XY',origin=(0,0,88))
r=w0.sketch().push([(-87,-89)]).rect(20,22).push([(-87,89)]).rect(20,22)
    .push([(88,-89)]).rect(20,22).push([(88,90)])
    .rect(20,20).finalize().extrude(-176)
    .union(w0.workplane(offset=-15/2).box(200,200,15))
```



```
import cadquery as cq
w0=cq.Workplane('XY',origin=(0,0,56))
w1=cq.Workplane('XY',origin=(0,0,26))
r=w0.workplane('XY',origin=(0,0,26))
r=w0.workplane(offset=-149/2).cylinder(149,18.5)
.union(w0.sketch().circle(100).circle(78,mode='s').finalize().extrude(-111))
.union(w1.workplane(offset=-52/2).cylinder(52,77))
.union(w1.workplane(offset=6/2).moveTo(97,0).box(3.5,9.5,6))
```

Figure 10: cadrille predictions on DeepCAD, Fusion360, and CC3D datasets. Each row contains predicted CadQuery Python code and its result after execution in Python interpreter.

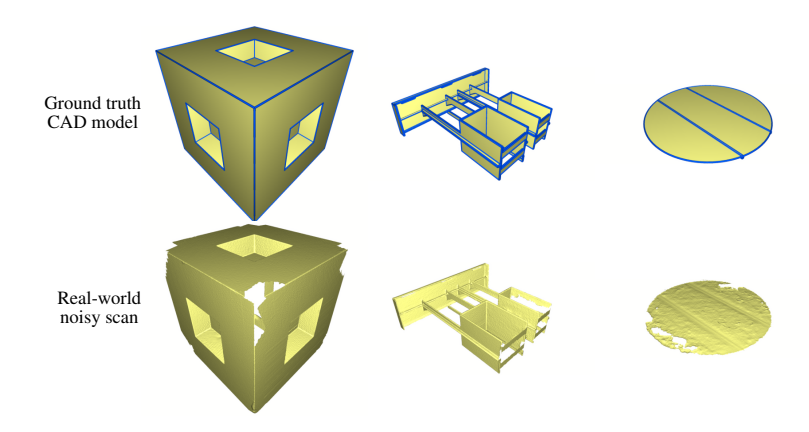


Figure 11: Ground truth CAD models (top row) and noisy scans (bottom row) from the real-world CC3D dataset.

Besides, CC3D contains generally more complex CAD models, which are constructed using operations beyond simple extrusion, including revolution, chamfer, and fillet.